Spray Deposition of Silver Nanowire Electrodes for Semitransparent Solid-State Dye-Sensitized Solar Cells

*George Y. Margulis, M. Greyson Christoforo, David Lam, Zach M. Beiley, Andrea R. Bowring, Colin D. Bailie, Alberto Salleo, and Michael D. McGehee**

Transparent top electrodes for solid-state dye-sensitized solar cells (ssDSCs) allow for fabrication of mechanically stacked ssDSC tandems, partially transparent ssDSCs for building integration, and ssDSCs on metal foil substrates. A solution-processed, highly transparent, conductive electrode based on PEDOT:PSS [poly(3,4-ethylenedioxythiophene):poly(styrenesulfonate)] and spray-deposited silver nanowires (Ag NWs) is developed as an effective top contact for ssDSCs. The electrode is solution-deposited using conditions and solvents that do not damage or dissolve the underlying ssDSC and achieves high performance: a peak transmittance of nearly 93% at a sheet resistance of 18 Ω/square – all without any annealing that would harm the ssDSC. The role of the PEDOT:PSS in the electrode is twofold: it ensures ohmic contact between the ssDSC 2,2′,7,7′-tetrakis-(*N*,*N*-di-p-methoxyphenylamine)9,9′-spirobifluorene (Spiro-OMeTAD) overlayer and the silver nanowires and it decreases the series resistance of the device. Semitransparent ssDSCs with D35 dye fabricated using this Ag NW/PEDOT:PSS transparent electrode show power conversion efficiencies of 3.6%, nearly as high as a reference device using an evaporated silver electrode (3.7%). In addition, the semitransparent ssDSC shows high transmission between 700–1100 nm, a necessity for use in efficient tandem devices. Such an electrode, in combination with efficient ssDSCs or hybrid perovskite-sensitized solar cells, can allow for the fabrication of efficient, cost-effective tandem photovoltaics.

G. Y. Margulis
Department of Applied Physics
Stanford University
Geballe Laboratory for Advanced Materials
476 Lomita Mall, Stanford, CA, 94305, USA
M. G. Christoforo
Department of Electrical Engineering
Stanford University
Geballe Laboratory for Advanced Materials
476 Lomita Mall, Stanford, CA, 94305, USA
D. Lam
Department of Physics
Stanford University
Geballe Laboratory for Advanced Materials
476 Lomita Mall, Stanford, CA, 94305, USA
Z. M. Beiley, A. R. Bowring, C. D. Bailie, Prof. A. Salleo, Prof. M. D. McGehee
Department of Materials Science and Engineering
Stanford University
Geballe Laboratory for Advanced Materials
476 Lomita Mall, Stanford, CA, 94305, USA
E-mail: mmcgehee@stanford.edu

DOI: 10.1002/aenm.201300660

1. Introduction

Solid-state dye-sensitized solar cells[1,2] (ssDSCs) have been developed as a stable alternative to dye-sensitized solar cells based on a liquid electrolyte and have achieved record efficiencies over 7%.[3] Solar cells using a similar structure, but sensitized using a hybrid organic-inorganic pervskite, termed meso-superstructured solar cells (MSSCs),[4–6] have attained efficiencies of over 12%.[7] Almost all MSSCs and ssDSCs are built on a fluorine-doped tin oxide (FTO)-glass transparent bottom electrode and use an evaporated metal layer for the hole-collecting top electrode. This architecture restricts ssDSCs and MSSCs to fabrication on glass substrates, requires illumination from the bottom electrode and only allows for fabrication of opaque solar cells. Development of a low-sheet resistance top electrode that can be deposited without damaging the underlying ssDSC or MSSC removes these restrictions and opens up the possibility of new device architectures.

Applying such a top electrode to make a semitransparent ssDSC allows for the use as a large bandgap solar cell in a tandem architecture. Since both ssDSCs and MSSCs have achieved open circuit voltages of over 1 V,[4,8,9] they are attractive candidates for large bandgap absorbers to be used in conjunction with a with low-bandgap absorber such as CIGS or Si.[10] In such a tandem device, an efficient semitransparent ssDSC must be fabricated with two transparent electrodes, allowing for unabsorbed low energy photons to pass through ssDSC and be absorbed in the lower bandgap solar cell.[10–15] In a similar architecture to a tandem device, upconverting materials can be used to expand the photoresponse of a semitransparent solar cell by absorbing sub-bandgap light passing through the device and re-emitting higher energy photons.[16–18] By themselves, semitransparent ssDSCs can be utilized in building-integrated photovoltaic windows. Additionally, the development of a transparent top electrode allows for fabrication of ssDSCs on opaque bottom substrates. Since ssDSCs require sintering at 450 °C, a temperature too high for most plastics, it is difficult to build flexible ssDSCs using the conventional architecture. With a transparent top electrode, ssDSCs can be roll-to-roll fabricated on metal foils,

allowing for easier deposition and processing, lower materials costs and flexible devices.

Previous efforts in fabricating a transparent top contact for ssDSCs have utilized a thin metal layer with sputtered tin-doped indium oxide (ITO),[19] but this electrode requires vacuum processing and has shown relatively high series resistance and low transmittance since ITO must be deposited at a low temperature to avoid damaging the organic hole transport material. Silver nanowires are a promising candidate for a top electrode in ssDSCs due to their high transparency, low sheet resistance and ability to be solution processed.[20–25] Silver nanowire meshes have achieved sheet resistances below 10 Ω/sq at transmittances of greater than 90% at 550 nm,[26] figures of merit necessary for incorporation into large-scale solar modules,[27,28] and have been incorporated in a variety of solar cells.[29–38] Typically, silver nanowires are deposited on glass, receive post-treatment such as annealing to optimize transmission and conductivity, and then are used as a bottom substrate for solar cell fabrication. However, deposition of silver nanowires on top of an ssDSC requires careful choice of deposition technique and parameters to prevent damage to the underlying device. As typical silver nanowire annealing temperatures (180 °C) cause rapid ssDSC degradation, the deposited silver nanowires must obtain low sheet resistances and high transmission without any annealing. Techniques such as fabricating the nanowires on a separate substrate and then transferring[39] using pressure and/or temperature often result in breakage of the ssDSC substrate. Finally, the silver nanowire electrode must make ohmic contact with the hole transport material, requiring deposition and optimization of a interfacial layer with low contact resistance, once again without damaging or dissolving the underlying device.

Here, we describe the fabrication of efficient ssDSCs using a completely solution-processed Ag NW/PEDOT:PSS electrode and analyze the optical and electronic properties of the device. These devices show efficiencies similar to those using an evaporated metal electrode, low series resistances, and allow for high transmittance of below-bandgap light. Such a transparent electrode should be compatible with other solar cells employing similar device structures such as MSSCs.

2. Device Architecture

2.1. Overview

A schematic of the device architecture is shown in **Figure 1**, along with scanning electron microscopy (SEM) images of the device cross section. The structure and fabrication procedure is exactly the same as a standard ssDSC except for the omission of the evaporated silver top electrode. Instead of this electrode, a conductive poly(3,4-ethylenedioxythiophene):poly(styrenesulfonate) (PEDOT:PSS layer; Clevios CPP-105D) is deposited by spin coating, followed by spray deposition of Ag NWs (donated by Blue Nano Inc.) from methanol. The CPP-105D formulation of PEDOT:PSS is used due to its ability to be deposited on hydrophobic surfaces and its relatively high conductivity. The PEDOT:PSS dispersion was diluted with isopropyl alcohol as it was found that the underlying Spiro-OMeTAD (2,2′,7,7′-tetrakis-(*N*,*N*-di-*p*-methoxyphenylamine)9,9′-spirobifluorene) layer is insoluble in most alcohols. Deposition of the PEDOT:PSS layer required sonication of the dispersion before spin coating, or agglomeration of the PEDOT:PSS in solution resulted in poor films. The CPP-105D formulation of PEDOT:PSS was also chosen for its resistance to dissolution by solvents; once the PEDOT:PSS layer was dried, it was not removed during subsequent nanowire deposition. It is difficult to measure the thickness of the PEDOT:PSS layer on the solar cell, as there is not enough contrast between the Spiro-OMETAD overlayer and the PEDOT:PSS interfacial layer in the SEM image (Figure 1d). However, the spin coating conditions used in making devices resulted in an 85-nm-thick PEDOT:PSS layer on a glass substrate. As discussed in subsequent sections, the purpose of the PEDOT:PSS layer is twofold: to allow for ohmic contact between the Spiro OMeTAD overlayer and the nanowire electrode, and to decrease the series resistance caused by lateral transport of charges between the nanowires.

Spray deposition of Ag NWs has been shown to produce uniform films of silver nanowires.[40] Here Ag NWs were deposited out of a methanol solution directly onto the PEDOT:PSS layer using a custom-built spray deposition system with a nitrogen gas driven atomizer nozzle. Solvent damage to the underlying Spiro-OMETAD layer can be eliminated during wire deposition by carefully choosing key deposition parameters (such as nozzle height, Ag NW solution flow rate and N_2 pressure) to minimize the amount of liquid solvent that reaches the device surface. Methanol was chosen as the solvent for the Ag NWs for its low boiling point, further reducing the amount of solvent reaching the device. While Spiro-OMeTAD and PEDOT:PSS are only minimally soluble in alcohols, solvent on the device may remove additives in the Spiro-OMeTAD, causing damage to the device. Heating during spray deposition was found to degrade the ssDSC and so spray deposition of the Ag NWs was done at room temperature. Ag NW mesh density (and thus

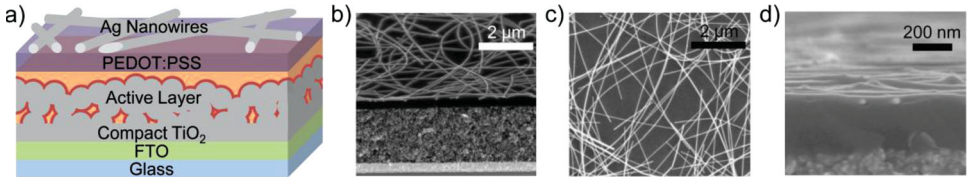

Figure 1. a) Schematic diagram of semitransparent ssDSC device. The device consists of a 400-nm-thick F:SnO_2 (FTO) layer, 100-nm-thick compact TiO_2 layer, 2-µm-thick dye-sensitized active layer, 200-nm-thick Spiro-OMeTAD overlayer, approximately 85-nm-thick PEDOT:PSS layer and solution deposited silver nanowires. b) SEM image of semitransparent ssDSC cross section at 20° angle of incidence. c) SEM image of Ag NW/PEDOT:PSS electrode at normal incidence. d) SEM image of the PEDOT:PSS/Ag NW composite electrode at 3° angle of incidence, showing that the wires are embedded in the PEDOT:PSS layer.

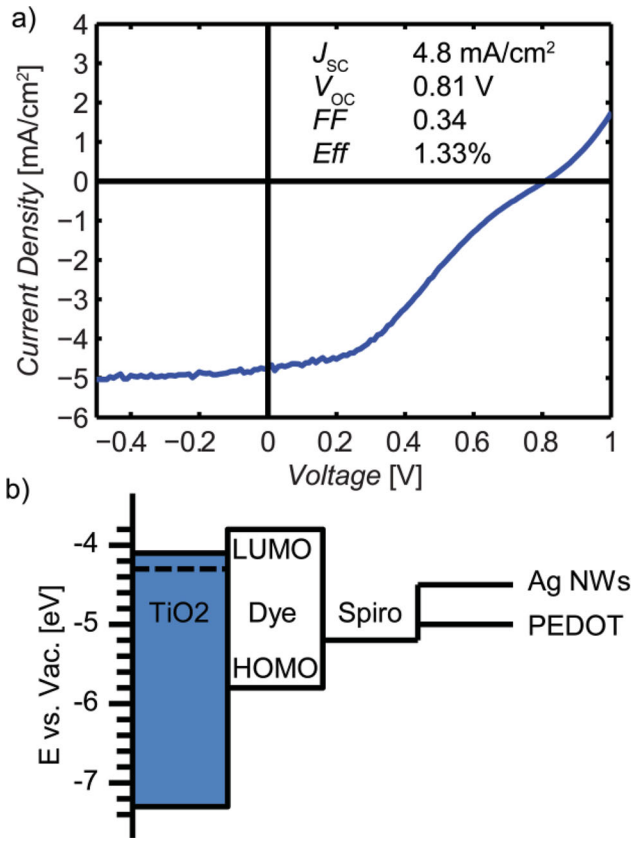

Figure 2. a) Current–voltage characteristics of ssDSC sensitized with D35 dye with no PEDOT:PSS interfacial layer. The *J–V* shows a distinctive s-shape, which causes a low fill factor (*FF*) and efficiency (*Eff*). b) Energy level diagram of ssDSC. The work functions of the Spiro-OMeTAD, PEDOT:PSS and Ag NWs were measured by PESA, while other energy levels are approximate and shown for comparison.

transmission and conductivity) is easily controlled by varying the concentration of wires in solution. As can be seen in Figure 1c, the silver nanowires form a sparse, uniform, well-dispersed mesh with maximum wire-to-wire gaps on the order of 1–2 µm. At higher magnification, it can be seen that the spray-deposited wires actually appear to embed into the PEDOT:PSS layer (Figure 1d), likely due to partial solvation of the PEDOT:PSS layer during spray deposition.

2.2. Role of the PEDOT:PSS Layer

The main purpose of the PEDOT:PSS interfacial layer is to ensure ohmic contact between the Spiro-OMeTAD and silver nanowires. As shown in **Figure 2**a, ssDSCs fabricated with no PEDOT:PSS layer display "s-shape" current–voltage characteristics, typically indicative of a barrier to charge transport.[41] Photoelectron spectroscopy in air (PESA) reveals that the work function of the as-sprayed nanowires is 4.5 eV (Figure S1 in the Supporting Information), while the work function of Spiro-OMeTAD is 5.2 eV (ssDSC energy level diagram depicted in Figure 2b). It is hypothesized that this energy level discrepancy is responsible for the energetic barrier seen in ssDSCs without an interfacial layer, and a more detailed discussion is provided in the Supporting Information. The work function of PEDOT:PSS was measured to be 5.0 eV, corresponding to a better energetic match with Spiro-OMeTAD. Thus the disappearance of the s-shape current–voltage characteristics observed when using an interfacial PEDOT:PSS layer may be attributed to the better work function match between PEDOT:PSS and Spiro-OMeTAD than between Spiro-OMeTAD and the as-sprayed silver nanowires.

A second important function of the PEDOT:PSS layer is to facilitate lateral charge transport in between the nanowires. While a four-point probe measurement quantifies the sheet resistance of charge transport through the nanowire mesh, photogenerated charges in the gaps between wires must first travel laterally to a nearby Ag NW before they can exit the device. As seen in Figure 1c, this distance can be on the order of 500 nm, meaning for low conductivity materials, the additional series resistance caused by lateral transport of charges to the nearest wire can be very significant. For very low conductivity materials, such as zinc oxide nanoparticles, it has even been seen that current is not collected far from the nanowires themselves, resulting in dead spots of low current.[42] In the case of more moderate conductivities, the resistance of lateral transport to the nanowire mesh results in additional solar cell series resistance causing a loss in fill factor. In the regime where the resistance of lateral transport does not cause dead spots, the photogenerated current can be assumed to be constant, and the power loss due to lateral transport can then be calculated for a given geometry of nanowires. For a 1D mesh of thin nanowires each evenly spaced a distance w apart, the power lost per unit area can be analytically calculated as

$$\frac{1}{12} J^2 w^2 R_s \tag{1}$$

where J is the photogenerated current density and R_s is the sheet resistance of the material in the gaps between the wires (units of Ω/square). Equation 1 allows for an estimate of the required interfacial material sheet resistance in order to have negligible losses due to lateral charge transport to the nanowires. Using a photogenerated current density, J, of 7 mA cm^{-2} and a distance, w, of 0.5 µm between nanowires, a R_s of approximately 1×10^9 Ω/square is required to ensure resistive losses are less than 0.1 mW cm^{-2} (or a 0.1% decrease in efficiency). This corresponds to the sheet resistance of a 500-nm-thick layer of Spiro-OMeTAD (conductivity of 2×10^{-5} Ω^{-1} cm^{-1}),[43] hence if Spiro-OMeTAD made ohmic contact to the Ag NWs, the losses in efficiency due to lateral transport would be relatively small: on the order of 0.1 mW cm^{-2}. However, for sparser nanowire meshes or other hole transport materials with lower conductivity (semiconducting polymer or small molecule hole transport materials with low doping densities),[43,44] these losses could be significantly higher. Hence, adding a highly conductive interfacial layer such as PEDOT:PSS (85 nm of Clevios CPP-105D PEDOT:PSS was measured to have a sheet resistance on the order of 10^5 Ω/square) will help eliminate any resistive losses due to lateral transport of photogenerated charge to the nanowires.

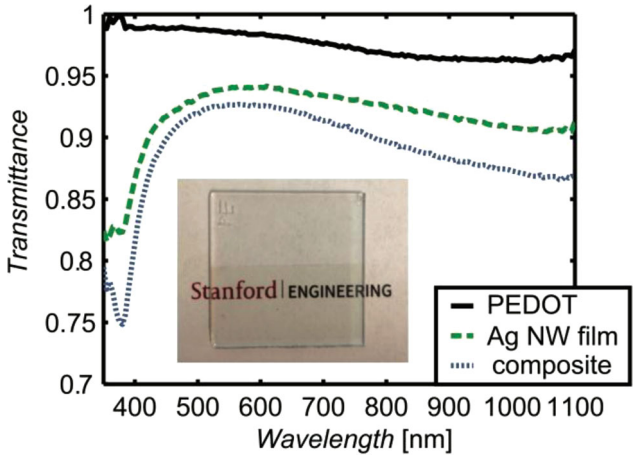

Figure 3. Transmittance of 85 nm PEDOT:PSS film, Ag NW film and Ag NW/PEDOT:PSS composite electrode. Inset: glass slide with Ag NW/PEDOT:PSS composite electrode on the bottom half of the glass substrate.

2.3. Electrode Characterization

The transmittance of the PEDOT:PSS/Ag NW composite electrode is shown in **Figure 3** along with an image of the electrode on glass. The electrode has a transmittance of over 90% between 450 and 700 nm and remains above 86% out to 1100 nm. This high transmittance is necessary for applications in tandem photovoltaics where the low bandgap device may absorb photons until 1100–1200 nm. The as-sprayed Ag NW mesh shows a peak transmittance of approximately 94% at a sheet resistance of 18 Ohm/square, some of the best figures of merit reported for Ag NW electrodes, even with no post-treatment such as annealing. Achieving such a low sheet resistance without any annealing[26,32] or additional post-processing[45] is made possible by the minimal amount of insulating surfactant on the surface of the silver nanowires in the formulation received from Blue Nano Inc. This allows for fabrication of conductive electrodes without damaging the underlying ssDSC with heat treatment typically required to remove surfactant. The sheet resistance of the PEDOT:PSS/Ag NW electrode was also measured when deposited on a ssDSC device (fabricated on glass with no conductive oxide), and resulted in similar values to that of the bare wires on glass (18 Ω/square). The density of wires can easily be adjusted to decrease the sheet resistance at the cost of transmittance. The PEDOT:PSS decreases the transmittance by only approximately 1–2% at 550 nm, but absorbs slightly more in the near infrared, causing a 4% drop in transmittance at 1100 nm.

3. Device Results

Devices were fabricated using D35, a commercially available, strongly absorbing organic dye (chemical structure shown in **Figure 4**b).[46] As seen in Figure 4c, the device has a bright red color due to its absorption in the green portion of the spectrum. Utilizing other color dyes can allow harvesting of other portions of the solar spectrum, along with desirable aesthetics for applications such as building-integrated photovoltaics. The current-voltage characteristics of the best-performing devices are shown in **Figure 5**, and the figures of merit are summarized in **Table 1**. While the open-circuit voltage (V_{oc}) and fill factor (FF) of the semitransparent ssDSC remains comparable to that of the reference device, the short-circuit photocurrent density (J_{sc}) drops slightly. The overall efficiency of the semitransparent device (3.6% under illumination from the FTO side) remained very close to that of the reference with an evaporated electrode (3.7%). Since record efficiencies of over 7% have been achieved with D-π-A dyes that have similar absorption spectra to D35, semitransparent ssDSCs using record-efficiency dyes can achieve efficiencies close to the 7% under FTO-side illumination.[3] Furthermore, MSSCs[4,7] sensitized with a strongly-absorbing perovskite could approach efficiencies of 12% using a PEDOT:PSS/Ag NW electrode, while still being transparent to sub-bandgap photons. Such a device would be an ideal high energy absorber in a tandem solar cell. This can be contrasted

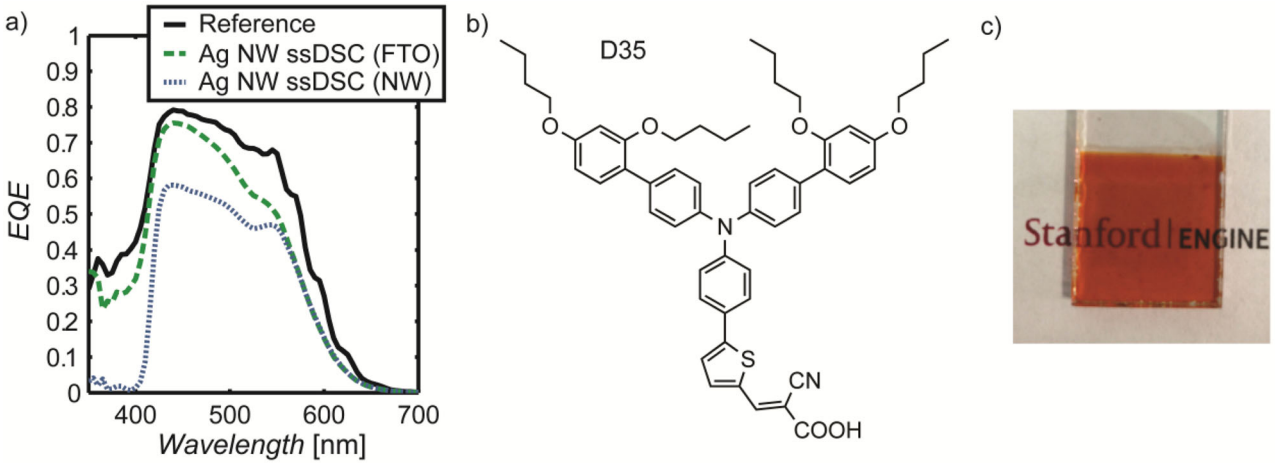

Figure 4. a) EQE of reference ssDSC device using an evaporated silver electrode and EQE of semitransparent ssDSC (using Ag NW/PEDOT:PSS electrode) illuminated from both the FTO and Ag NW electrodes. b) Chemical structure of D35 dye used in device fabrication. c) Picture of semitransparent ssDSC. The Ag NW/PEDOT:PSS electrode is barely visible as a slightly darker square in the middle of the device.

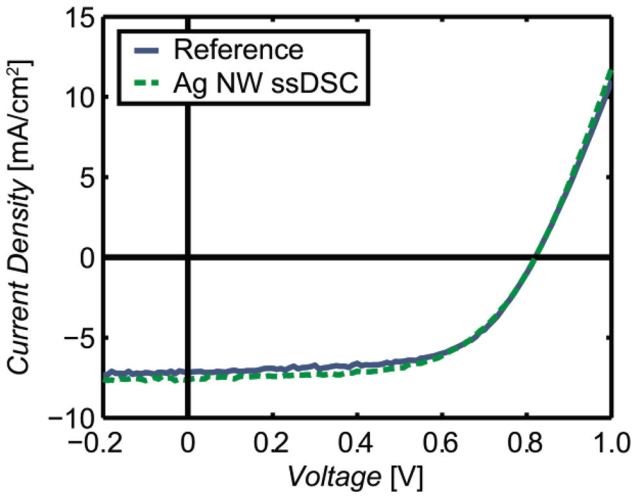

Figure 5. *J–V* curves of best semitransparent ssDSC and best reference device using an evaporated silver electrode. The difference in current between devices is only 0.3 mA cm^{-2}, which is slightly less than typical between a reference device and a semitransparent device. Device area was approximately 0.5 cm^2 and was masked with a 0.2 cm^2 mask. Even for small areas (0.1 cm^2), references in our lab are less than 4.0% efficient.

with organic solar cells, where the weaker absorption of the device means that semitransparent cells achieve significantly lower efficiencies than those with a reflective back electrode.[31,33,37] As can be seen in Figure 4a, the external quantum efficiency, or EQE, of the semitransparent device is nearly as high as that of the reference, particularly at the dye's peak absorption. Additionally, it should be noted that these devices were fabricated with a moderate-size active area (electrode area of approximately 0.5 cm^2), and utilizing a spray-deposited semitransparent electrode resulted in a higher device yield with less shorting than in ssDSCs fabricated with a standard evaporated silver electrode. This is likely due to PEDOT:PSS and Ag NWs being less likely to short the device through pinholes than the silver evaporation. As shown in Table 1, the measured series resistances of the *J–V* curves were nearly identical, showing that the additional series resistance of the silver nanowire electrode is not a significant loss. The series resistance in these ssDSCs is dominated by other components, such as the internal resistance of the device and Spiro-OMeTAD overlayer.

While semitransparent devices illuminated from the F:SnO_2 (FTO) electrode showed efficiencies comparable to those of reference devices, various device architectures, such as ssDSCs on metal substrates, would require that incoming light be incident through the Ag NW electrode. Because incoming light is filtered by the Spiro-OMeTAD overlayer before it can be absorbed by the dye, the EQE drops to nearly 0 below 425 nm where Spiro-OMeTAD is strongly absorbing (Figure 4a). Furthermore, there is an additional loss in photoresponse between 425–550 nm, which can be attributed to the parasitic absorption of the oxidized Spiro-OMeTAD species in the overlayer.[47–50] Beyond 550 nm, the EQE of the semitransparent ssDSC is the same when illuminated from either side, due to the fact that the optical performance of the Ag NW/PEDOT:PSS electrode is comparable to that of the FTO. Overall, illumination from the Ag NW electrode side results in approximately a 20% drop in integrated short-circuit photocurrent, primarily due to the effects of the Spiro-OMeTAD overlayer.

One of the primary motivations for making semitransparent ssDSCs is for use as a top cell in tandem devices with a silicon or copper indium gallium selenide (CIGS) low bandgap bottom cell. In such a hybrid tandem photovoltaic (HTPV),[10] the incident light would first pass through the semitransparent cell, where the high energy photons would be absorbed, and the remaining photon flux would be absorbed by the low bandgap inorganic solar cell. In order to achieve an efficient HTPV device, the semitransparent top cell must strongly absorb photons with energy above its bandgap, but must show a transmittance of approximately 80% or more for lower energy photons.[10] The transmittance, absorptance, and reflectance of the semitransparent ssDSC are quantified in **Figure 6**. As can be seen, a majority of the photons below 550 nm are absorbed within the device, while above the bandgap of the dye the transmittance peaks at 74% at 820 nm, with an average transmittance of 67% between 700 and 1100 nm. A significant amount of this loss in the infrared portion of the spectrum can be attributed to the strong absorption of the soda-lime glass substrate,

Table 1. Photovoltaic figures of merit for best-performing semitransparent ssDSC and reference device using an evaporated Ag electrode under simulated AM 1.5G illumination.

Device	J_{SC} [mA cm^{-2}]	V_{OC} [V]	Fill Factor	Efficiency [%]	Series Resistance[a)] [Ω cm^2]
Reference	7.6	0.82	0.60	3.7	13.8
NW device	7.2	0.82	0.61	3.6	15.1

[a)]Based on a linear fit of the *J–V* curve in light at a forward bias of 0.91–1.00 V.

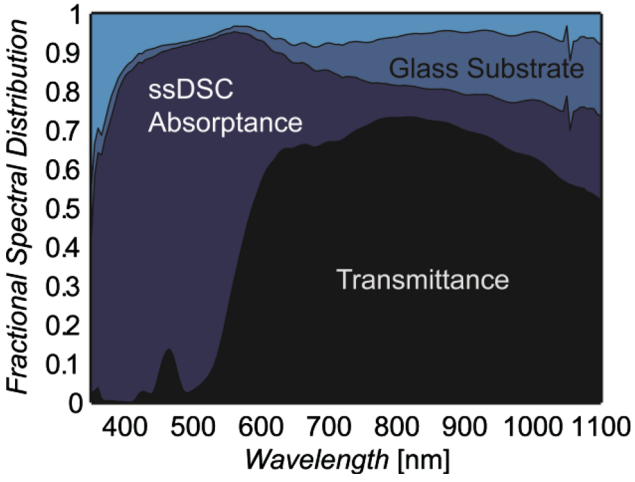

Figure 6. Fractional spectral distribution of incident light upon the semitransparent ssDSC. Shown is the fraction of photons transmitted through the semitransparent ssDSC (all layers other than glass substrate, including the FTO), the fraction absorbed by the semitransparent ssDSC, and the fraction absorbed by the soda-lime glass substrate. The light area at the top of the plot denotes reflected photons. Transmittance and absorptance measurements were carried out using an integrating sphere to account for scattering.

which absorbs approximately 18% of incident 1100 nm photons. The actual absorptance of the semitransparent ssDSC (every layer other than glass substrate) is only 10–22% between 700 and 1100 nm, suggesting that with more transparent glass and an antireflective coating, such a semitransparent cell could achieve the transmission levels necessary for use in a HTPV.

4. Conclusions

Transparent top electrodes for ssDSCs have a variety of applications ranging from tandem devices to photovoltaic windows. We have developed a method to spray a silver nanowire/PEDOT:PSS electrode which achieves greater than 92% peak transmittance without damaging the underlying ssDSC. The use of a PEDOT:PSS interfacial layer allows the Ag NWs to make ohmic contact to the Spiro-OMeTAD overlayer. Additionally, the PEDOT:PSS layer eliminates any contribution to the series resistance caused by lateral transport of charges between nanowires. Combining this electrode with a D35-sensitized ssDSC, we have been able to make an aesthetically appealing, transparent device with an efficiency of 3.6%, only 0.1% less than the efficiency of standard D35 ssDSCs using an evaporated silver electrode. The semitransparent device shows high transmission below the device bandgap, a requirement for fabrication of efficient hybrid tandem photovoltaics. Development of such highly transparent Ag NW-based electrodes for ssDSCs and MSSCs are an important step in the realization of HTPV devices that can exceed 20% efficiency and provide clean energy at competitive prices.

5. Experimental Section

ssDSC Device Fabrication: FTO substrates (TEC15, Hartford Glass Co.) were cleaned by sonication in Extran detergent, acetone and isopropyl alcohol, with subsequent UV-ozone treatment for 20 min. A compact TiO_2 layer (50–100 nm) was deposited using spray pyrolysis of titanium diisopropoxide bis(acetylacetonate) (Aldrich 75 wt% in isopropyl alcohol, diluted 10× with isopropyl alcohol) on the FTO substrate. The mesoporous titania layer was deposited by doctorblading titania nanoparticles dispersed in paste. Dyesol paste (NR-18T) diluted with terpinoel 1:1 (by weight) was used, resulting in nanoparticle films with thicknesses of approximately 2.2 µm. Films were subsequently sintered at 500 °C for 30 min on a hotplate. Titania nanoparticle films were then immersed in $TiCl_4$ solution overnight and then heated to 500 °C for 30 min once again. The substrates were then sensitized by immersion for 18 h in a 0.2 mm solution of D35 dye (Dyenamo) in ethanol.

Spiro-OMeTAD solution contained tert-butylpyridine (4-tbp), Spiro-OMeTAD (Luminescence Technology corporation), and lithium bis(trifluoromethylsulfonyl)imide salt (Li-TFSI) (pre-solved in acetonitrile in 170 mg mL-1). Spiro solution was made by taking a 1g Spiro-OMeTAD: 97 mL 4-tbp: 208 mL Li-TSFI solution mixture dissolved in chlorobenzene (with 225 mg Spiro-OMeTAD/1 mL chlorobenzene). The Spiro-OMeTAD solution was then infiltrated into the sensitized nanoparticle film by spincoating at 2000 rpm. After allowing the device to dry for 18 h in a dry air environment, the top electrode was deposited. The electrode area was first masked off by polyimide tape and the tape removed after electrode deposition. In the case of the evaporated silver reference device, a 200 nm silver cathode was deposited by thermal evaporation (10^{-6} Torr pressure). In the case of the semitransparent device, the electrode was deposited as described below.

Ag NW/PEDOT:PSS Electrode Fabrication: PEDOT:PSS from Heraeus (formulation Clevios CPP-105D) was diluted 1:1 (by volume) with isopropyl alcohol and deposited by spincoating at 4000 rpm on the device or film. The device/film was then allowed to dry in a dry air environment for 5 h. Silver nanowires, 10–30 µm long and 30–50 nm in diameter were provided by Blue Nano Inc. in a 10 mg mL^{-1} ethanol solution. This solution was diluted to 5 mg Ag per mL ethanol for long term storage and further diluted with methanol to 0.11 mg mL^{-1} for spray deposition. 45 mL of this solution was loaded into a Harvard apparatus PhD Ultra syringe pump and delivered to a 1/4JN-SS+SU11DF-SS atomizing nozzle by Spray Systems Co. at a rate of 4 mL min^{-1}. Nitrogen gas at 25 psi was delivered to the nozzle. The nozzle was positioned 110 mm above a motorized, computer controlled X-Y stage (Parker Hannafin ProMECH LP28) onto which the ssDSC devices were taped. To ensure uniformity and repeatability of the deposited electrodes, the X-Y stage moved the devices under the nozzle at a rate of 20 cm s^{-1} during the entire spray process such that the nozzle sprayed uniformly over a 20 cm × 5.5 cm area. This way 10 devices at a time could receive identical nanowire coatings.

4-Point Probe Measurements: Electrode sheet resistance was measured using an in-line four-point probe with 1 mm tip spacing by Jandel Engineering connected to a Kiethley 2400 sourcemeter. Each measurement consisted of recording 100 pairs of current and voltage data points between –30 and 30 mV and checking that each pair corresponded to the same sheet resistance. While the sheet resistance of the silver nanowire mesh on glass was measured to be 18 Ω/square, the corresponding sheet resistance of the composite PEDOT:PSS/Ag NW electrode on glass was unable to be measured with a 4-point-probe (readings of 4–8 kΩ/square). However, 4-point-probe measurements of the Ag NW/PEDOT:PSS electrode on a ssDSC (fabricated without an FTO layer to avoid shorted measurement of the FTO sheet resistance) found sheet resistances of approximately 18 Ω/square.

J–V Measurements: All devices were subject to 5 min light soaking under simulated AM 1.5G spectrum before measurement. *J–V* curves were taken with a Keithley 2400 sourcemeter, under simulated AM 1.5G illumination using a Spectraphysics model 91160 solar simulator calibrated with a hamamatsu Si photodiode with KG5 filter. The ssDSC was was masked with a 0.2 cm^2 area machined mask during *J–V* measurements to ensure accurate illumination area.

EQE, Transmittance, and Absorptance Measurements: External quantum efficiency measurements were performed at a chopping rate of 40 Hz with a white light illumination bias of approximately 0.4 suns applied using a white light LED array powered by a DC power source. A Newport Apex monochromator illuminator was used (in conjunction with a Princeton Instruments monochromator and a filter wheel) to generate the monochromated, chopped signal. The current response of the ssDSC was put through a 1000 Ω transimpedance amplifier and recorded using a Stanford Instruments lock-in amplifier. Calibration of the EQE measurement was performed using a calibrated photodiode of known EQE. Additionally, the monochromated EQE signal was split with a 50:50 beam splitter into a second reference photodiode connected to another Stanford Instruments lock-in amplifier that was used to correct for any fluctuations in the EQE beam source intensity.

Absorptance and transmittance measurements were performed using the same light source/monochromator as the EQE measurements and measured using an integrating sphere with an attached silicon photodiode. For measuring transmittance, the device/film was placed in front of the integrating sphere such that only light passing through the device/film would be measured. For absorptance, the device was placed in the center of the integrating sphere, allowing for a measurement of the sum of the transmittance and reflectance. The reflectance was then calculated by 1 – (transmittance + absorptance).

SEM Images: Device images were taken using a FEI XL30 Sirion SEM. The ssDSC was cracked in half and placed on SEM sample mounts of various tilt angle (0°, 20°, 90°) using graphite paste.

PESA Measurements: Samples for PESA measurements were prepared using identical spin coating or spraying conditions as during device fabrication but on a glass substrate. PESA spectra were measured using a Riken Keiki AC-2 photoelectron spectrometer.

Supporting Information

Supporting Information is available from the Wiley Online Library or from the author.

Acknowledgements

G. Y. M. and M. G. C. contributed equally to this work. This work was supported by the Office of Naval Research (ONR) under grant N000141110244. This material was also based upon work supported by the Department of Energy through the Bay Area Photovoltaic Consortium under Award Number DE-EE0004946. G.Y.M. would like to acknowledge funding from the TomKat Center for Sustainable Energy. The nanowire electrode fabrication work was performed in part at the Stanford Nanofabrication Facility's nSiL lab which was funded by National Science Foundation award ARI-0963061. Silver nanowires were donated by Blue Nano Inc.

Received: June 13, 2013
Published online: July 23, 2013

[1] U. Bach, D. Lupo, P. Comte, J. E. Moser, F. Weissörtel, J. Salbeck, H. Spreitzer, M. Grätzel, *Nature* **1998**, *395*, 583.
[2] C.-Y. Hsu, Y.-C. Chen, R. Y.-Y. Lin, K.-C. Ho, J. T. Lin, *Phys. Chem. Chem. Phys.* **2012**, *14*, 14099.
[3] J. Burschka, A. Dualeh, F. Kessler, E. Baranoff, N.-L. Cevey-Ha, C. Yi, M. K. Nazeeruddin, M. Grätzel, *J. Am. Chem. Soc.* **2011**, *133*, 18042.
[4] M. M. Lee, J. Teuscher, T. Miyasaka, T. N. Murakami, H. J. Snaith, *Science* **2012**, *338*, 643.
[5] H.-S. Kim, C.-R. Lee, J.-H. Im, K.-B. Lee, T. Moehl, A. Marchioro, S.-J. Moon, R. Humphry-Baker, J.-H. Yum, J. E. Moser, M. Grätzel, N.-G. Park, *Sci. Rep.* **2012**, *2*, 1.
[6] I. Chung, B. Lee, J. He, R. P.H. Chang, M. G. Kanatzidis, *Nature* **2012**, *485*, 486.
[7] J. H. Noh, S. H. Im, J. H. Heo, T. N. Mandal, S. Il Seok, *Nano Lett.* **2013**, *13*, 1764.
[8] P. Chen, J. H. Yum, F. De Angelis, E. Mosconi, S. Fantacci, S.-J. Moon, R. H. Baker, J. Ko, M. K. Nazeeruddin, M. Grätzel, *Nano Lett.* **2009**, *9*, 2487.
[9] E. Edri, S. Kirmayer, D. Cahen, G. Hodes, *J. Phys. Chem. Lett.* **2013**, *4*, 897.
[10] Z. M. Beiley, M. D. McGehee, *Energ. Environ. Sci.* **2012**, *5*, 9173.
[11] P. Liska, K. R. Thampi, M. Grätzel, D. Brémaud, D. Rudmann, H. M. Upadhyaya, A. N. Tiwari, *Appl. Phys. Lett.* **2006**, *88*, 203103.
[12] S. Wenger, S. Seyrling, A. N. Tiwari, M. Grätzel, *Appl. Phys. Lett.* **2009**, *94*, 173508.
[13] S. Ito, I. M. Dharmadasa, G. J. Tolan, J. S. Roberts, G. Hill, H. Miura, J.-H. Yum, P. Pechy, P. Liska, P. Comte, M. Grätzel, *Sol. Energy* **2011**, *85*, 1220.
[14] W.-S. Jeong, J.-W. Lee, S. Jung, J. H. Yun, N.-G. Park, *Sol. Energy Mater. Sol. Cells* **2011**, *95*, 3419.
[15] Z. Tang, Z. George, Z. Ma, J. Bergqvist, K. Tvingstedt, K. Vandewal, E. Wang, L. M. Andersson, M. R. Andersson, F. Zhang, O. Inganäs, *Adv. Energy Mater.* **2012**, *2*, 1467.
[16] W. Zou, C. Visser, J. A. Maduro, M. S. Pshenichnikov, J. C. Hummelen, *Nat. Photonics* **2012**, *6*, 1.
[17] S. Fischer, J. C. Goldschmidt, P. Löper, G. H. Bauer, R. Brüggemann, K. Krämer, D. Biner, M. Hermle, S. W. Glunz, *J. Appl. Phys.* **2010**, *108*, 044912.
[18] X. Huang, S. Han, W. Huang, X. Liu, *Chem. Soc. Rev.* **2013**, *42*, 173.
[19] Y.-F. Chiang, C.-H. Tsai, P. Chen, T.-F. Guo, *Sol. Energy* **2012**, *86*, 1967.
[20] J.-Y. Lee, S. T. Connor, Y. Cui, P. Peumans, *Nano Lett.* **2008**, *8*, 689.
[21] S. De, T. M. Higgins, P. E. Lyons, E. M. Doherty, P. N. Nirmalraj, W. J. Blau, J. J. Boland, J. N. Coleman, *ACS Nano* **2009**, *3*, 1767.
[22] L. Hu, H. S. Kim, J. Lee, P. Peumans, Y. Cui, *ACS Nano* **2010**, *4*, 2955.
[23] R. Zhu, C.-H. Chung, K. C. Cha, W. Yang, Y. B. Zheng, H. Zhou, T.-B. Song, C.-C. Chen, P. S. Weiss, G. Li, Y. Yang, *ACS Nano* **2011**, *5*, 9877.
[24] W. Gaynor, G. F. Burkhard, M. D. McGehee, P. Peumans, *Adv. Mater.* **2011**, *23*, 2905.
[25] T. Kim, Y. W. Kim, H. S. Lee, H. Kim, W. S. Yang, K. S. Suh, *Adv. Funct. Mater.* **2013**, *23*, 1250.
[26] J. Krantz, M. Richter, S. Spallek, E. Spiecker, C. J. Brabec, *Adv. Funct. Mater.* **2011**, *21*, 4784.
[27] M. W. Rowell, M. D. McGehee, *Energ. Environ. Sci.* **2011**, *4*, 131.
[28] J. D. Servaites, S. Yeganeh, T. J. Marks, M. A. Ratner, *Adv. Funct. Mater.* **2010**, *20*, 97.
[29] A. Kim, Y. Won, K. Woo, C.-H. Kim, J. Moon, *ACS Nano* **2013**, *7*, 1081.
[30] J. Huang, G. Li, Y. Yang, *Adv. Mater.* **2008**, *20*, 415.
[31] J. Krantz, T. Stubhan, M. Richter, S. Spallek, I. Litzov, G. J. Matt, E. Spiecker, C. J. Brabec, *Adv. Funct. Mater.* **2013**, *23*, 1711.
[32] W. Gaynor, J.-Y. Lee, P. Peumans, *ACS Nano* **2010**, *4*, 30.
[33] J.-Y. Lee, S. T. Connor, Y. Cui, P. Peumans, *Nano Lett.* **2010**, *10*, 1276.
[34] D.-S. Leem, A. Edwards, M. Faist, J. Nelson, D. D. C. Bradley, J. C. de Mello, *Adv. Mater.* **2011**, *23*, 4371.
[35] A. Colsmann, A. Puetz, A. Bauer, J. Hanisch, E. Ahlswede, U. Lemmer, *Adv. Energy Mater.* **2011**, *1*, 599.
[36] C. Chen, L. Dou, R. Zhu, C. Chung, T. Song, Y. B. Zheng, S. Hawks, G. Li, P. S. Weiss, Y. Yang, *ACS Nano* **2012**, *6*, 7185.
[37] F. Guo, X. Zhu, K. Forberich, J. Krantz, T. Stubhan, M. Salinas, M. Halik, S. Spallek, B. Butz, E. Spiecker, T. Ameri, N. Li, P. Kubis, D. M. Guldi, G. J. Matt, C. J. Brabec, *Adv. Energy Mater.* **2013**, DOI: 10.1002/aenm.201300100.
[38] M. Al-Mamun, J.-Y. Kim, Y.-E. Sung, J.-J. Lee, S.-R. Kim, *Chem. Phys. Lett.* **2013**, *561–562*, 115.
[39] B. E. Hardin, W. Gaynor, I.-K. Ding, S.-B. Rim, P. Peumans, M. D. McGehee, *Org. Electron.* **2011**, *12*, 875.
[40] V. Scardaci, R. Coull, P. E. Lyons, D. Rickard, J. N. Coleman, *Small* **2011**, *7*, 2621.
[41] W. Tress, S. Pfuetzner, K. Leo, M. Riede, *J. Photonics Energy* **2011**, *1*, 011114.
[42] F. S. F. Morgenstern, D. Kabra, S. Massip, T. J. K. Brenner, P. E. Lyons, J. N. Coleman, R. H. Friend, *Appl. Phys. Lett.* **2011**, *99*, 183307.
[43] T. Leijtens, I.-K. Ding, T. Giovenzana, J. T. Bloking, M. D. McGehee, A. Sellinger, *ACS Nano* **2012**, *6*, 1455.
[44] W. Zhang, Y. Cheng, X. Yin, B. Liu, *Macromol. Chem. Phys.* **2011**, *212*, 15.
[45] E. C. Garnett, W. Cai, J. J. Cha, F. Mahmood, S. T. Connor, M. Greyson Christoforo, Y. Cui, M. D. McGehee, M. L. Brongersma, *Nat. Mater.* **2012**, *11*, 241.
[46] X. Jiang, K. M. Karlsson, E. Gabrielsson, E. M. J. Johansson, M. Quintana, M. Karlsson, L. Sun, G. Boschloo, A. Hagfeldt, *Adv. Funct. Mater.* **2011**, *21*, 2944.
[47] G. Y. Margulis, B. E. Hardin, I.-K. Ding, E. T. Hoke, M. D. McGehee, *Adv. Energy Mater.* **2013**, DOI: 10.1002/aenm.201300057.
[48] U. B. Cappel, T. Daeneke, U. Bach, *Nano Lett.* **2012**, *12*, 4925.
[49] A. Abate, T. Leijtens, S. Pathak, J. Teuscher, R. Avolio, M. E. Errico, J. Kirkpatrik, J. M. Ball, P. Docampo, I. McPherson, H. J. Snaith, *Phys. Chem. Chem. Phys.* **2013**, *15*, 2572.
[50] S. Fantacci, F. De Angelis, M. K. Nazeeruddin, M. Grätzel, *J. Phys. Chem. C* **2011**, *115*, 23126.